Journal of Biomedical Optics

SPIEDigitalLibrary.org/jbo

Visualization of the solubilization process of the plasma membrane of a living cell by waveguide evanescent field fluorescence microscopy

Abdollah Hassanzadeh
Heun Kan Ma
S. Jeffrey Dixon
Silvia Mittler

SPIE

Visualization of the solubilization process of the plasma membrane of a living cell by waveguide evanescent field fluorescence microscopy

Abdollah Hassanzadeh,[a*] Heun Kan Ma,[a,b] S. Jeffrey Dixon,[b] and Silvia Mittler[a]
[a]Western University, London, Department of Physics and Astronomy, Ontario, Canada
[b]Western University, London, Department of Physiology and Pharmacology, Schulich School of Medicine and Dentistry, Ontario, Canada

Abstract. Waveguide evanescent field fluorescence microscopy (WEFF) is a novel microscopy technology that allows imaging of a cell's plasma membrane in the vicinity of a glass substrate with high axial resolution, low background and little photobleaching. Time-lapse imaging can be performed to investigate changes in cell morphology in the presence or absence of chemical agents. WEFF microscopy provides a method to investigate plasma membranes of living cells and allows a comparison to simplified model membranes immobilized on planar substrates. The interaction of the nonionic detergent Triton X-100 with plasma membranes of osteoblasts in an aqueous environment was investigated. Solubilization of the membranes very close to the waveguide surface was visualized and related to the three-stage solubilisation model proposed for liposomes and supported lipid bilayers. Findings for the plasma membranes of cells are in excellent agreement with results reported for these artificial model systems.
 [DOI: 10.1117/1.JBO.17.7.076025]

Keywords: cell membrane; fluorescence microscopy; optical waveguide; evanescent field; Triton X-100; solubilization; detergent-membrane interaction.

Paper 12094 received Feb. 9, 2012; revised manuscript received May 24, 2012; accepted for publication Jun. 1, 2012; published online Jul. 24, 2012.

1 Introduction

Cells are fundamental units of life that move, grow, divide and respond to their environment.[1] The lipid bilayer, which forms the membranes around and within a cell, is a two-dimensional self-assembled structure containing hundreds of different lipids and proteins.[2] Detergents are commonly used agents in membrane research. They have been used for isolation,[3] purification,[4] reconstitution of proteins,[3] permeabilization or perturbation of membrane structure,[5] and preparation and solubilization of liposomes.[3] Not only has solubilization by detergents played an important role in biomembrane research, but also the resistance of some parts of the membrane to detergents has provided evidence for the existence of lipid domains or rafts in cell membranes.[6,7]

Detergent-membrane interactions have been the subject of many studies.[6–19] Functional membranes typically exist in the fluid state also called the liquid-disordered state.[20] Due to the difficulties of working with authentic cell membranes, simplified membrane models—such as supported lipid bilayers, liposome mimicking biological systems or phosphatidylcholine bilayers—have often been used to investigate detergent-membrane interactions.[7] Model membranes were helpful in exploring the basic membrane functions. However, in comparison to a living cell—with integral and peripheral proteins, cholesterol molecules and oligosaccharides in and on their plasma membrane—artificial membrane models cannot mimic all aspects of plasma membrane function. In addition, studying the interaction between lipids and detergents in the form of vesicles (liposomes) or supported lipid bilayers has several other disadvantages. For example, in supported lipid bilayers, the quality of the deposited film plays a major role. In addition, direct contact with the underlying substrate affects the bilayer's structure and fluidity, and blocks access of solutions to both sides of membrane.

A number of studies have been performed to understand the principles governing lipid-detergent interactions using liposomes or supported lipid bilayers as simplified membrane models. Commonly employed experimental techniques are light scattering,[11,21–33] turbidimetry,[11,21,28] centrifugation,[4] electron microscopy (EM),[26–28,34,35] atomic force microscopy (AFM),[10] two-photon fluorescence microscopy and spectroscopy,[7] waveguide light mode spectroscopy,[36] magnetic resonance spectroscopy,[11,25,33] nuclear magnetic resonance,[11] and fluorescence anisotropy and spectroscopy.[8,11]

The results of lipid-detergent interaction studies using the above mentioned techniques have been related to a three-stage model, which was described by Lichtenberg et al.[8] and verified by various microscopy and spectroscopy techniques. In stage I, with increasing detergent concentration, detergent incorporates into the bilayer. At this stage, solubilization does not occur, but the bilayer becomes saturated with detergent. However, changes in the size and structure of vesicles were observed with microscopic techniques such as transmission electron microscopy, AFM, and EM.[10,26–28,34,35] At stage II, with further increase in detergent concentration, the bilayer starts to solubilise. Lipid vesicles saturated with detergent form and coexist with mixed micelles of lipid and detergent. At stage III, the entire membrane solubilises, and only mixed micelles exist.[36,37]

*Present address: University of Kurdistan, Department of Physics, Sanandaj, Kurdistan, Iran.

Address all correspondence to: Silvia Mittler, Western University, London, Department of Physics and Astronomy, Ontario, Canada. Tel: +1 (519) 661-2111 loc. 88592; Fax: +1 (519) 661-2033; E-mail: smittler@uwo.ca

0091-3286/2012/$25.00 © 2012 SPIE

In the present work, we applied a recently introduced evanescent microscopy technique, waveguide evanescent field fluorescence (WEFF) microscopy.[38–44] Simple slab waveguides were used as substrates to image and observe plasma membrane solubilisation with Triton X-100 in real time. Triton X-100 [$C_{14}H_{22}O(C_2H_4O)_n$] is a nonionic surfactant which has a hydrophilic polyethylene oxide chain (on average it has 9.5 ethylene oxide units) and an aromatic hydrocarbon hydrophobic group. It is commonly used in biochemical applications including membrane permeabilization and cell lysis. Moreover, Triton X-100 is a relatively mild detergent which does not denature most proteins.[37,45]

WEFF microscopy detects fluorescence dye distribution only within the first 70 nm above a waveguide surface. This technique not only allows time-lapse imaging, but also offers a high axial resolution, very high signal to noise ratio and negligible photobleaching.[40–44] In all evanescent techniques, a thin film of light, having a high intensity directly at the interface and decaying exponentially away from the interface, is applied to the sample. Other evanescent waveguide techniques have been used to investigate cell-substratum interactions as well; however, these studies did not necessarily involve the use of fluorescent dyes or the acquisition of images. Most of these methods (e.g., reverse waveguides,[46] optical EPIC systems[47]) measure refractive index changes. For example Cottier et al., have investigated the coupling behaviour of a laser beam into a waveguide mode when cells are present on the grating and could determine a characteristic length of a cell perturbation.[48] Aref et al., have investigated the changes in refractive index occurring when a stem cell secretes macromolecules onto a waveguide surface.[49]

Both label-free methods and fluorescent dyes have been used to study cell-substrate interactions, leading to different sets of information. Label-free methods typically investigate the optical thickness, a convolution of the local refractive index architecture and the film thickness on the waveguide; whereas fluorescence methods rely on photons emitted by the fluorescent probes. The number of emitted photons depends not only on the amount of dye present, but also on the local conditions of the dye, its quantum yield depending on its environment. For instance, an alteration in quantum yield due to a change in quenching can give concentration information, which cannot be obtained from refractive index data. Thus, for some applications, the fluorescence signal contains more information than a change in the refractive index architecture. In such cases, a method employing a label is advantageous.

A scheme of WEFF microscopy is depicted in Fig. 1. The key element of WEFF microscopy is an optical waveguide carrying an evanescent field. An optical waveguide consists of: (i) a high refractive index, thin film (in the order of μm thickness) guiding the light; (ii) a substrate, acting as the supporting material onto which the waveguide is deposited; and (iii) a medium covering the entire structure. To couple a laser beam into the waveguide, a grating needs to be fabricated on the waveguide surface or embedded into it. When a laser beam is incident onto the grating at a waveguide mode resonance angle, light couples into the waveguide and propagates along the waveguide. The guided light in the waveguide generates an evanescent field. This thin film of light—the intensity of which decays exponentially into the cover medium—can be used as an illumination source to excite

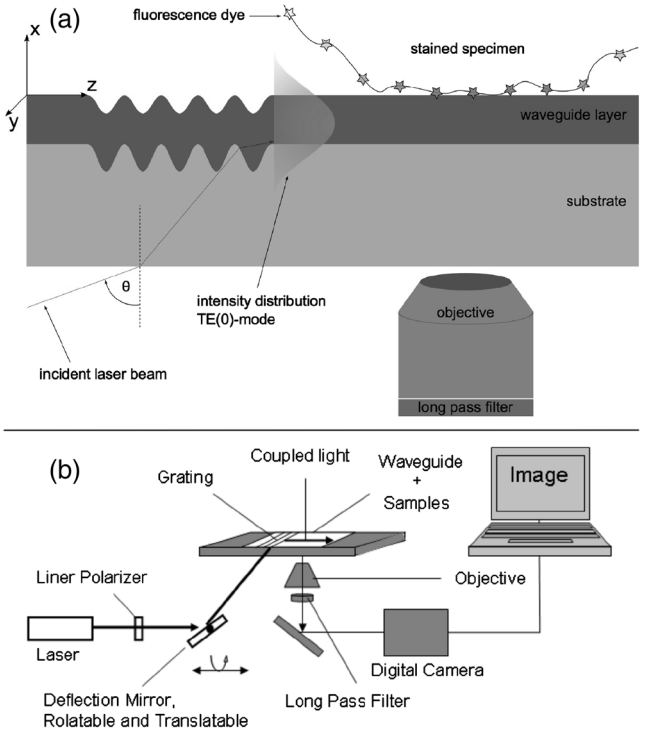

Fig. 1 (a) Scheme of the waveguide with cell and guided electro-magnetic field. (b) Scheme of the entire WEFF microscope.

fluorophores. Photons emitted from excited fluorophores are collected by the objective of an inverted microscope. Since in WEFF microscopy only a thin film of the sample is illuminated by the evanescent field (in the present case 70 nm), the captured images show only details within this short distance above the substrate. This makes WEFF microscopy a powerful technique to visualize and quantify dynamics of biological interface phenomena in an aqueous environment.[40–44,50,51]

Cell adhesion structures (such as focal adhesions) mediate mechanical and signaling interactions between cells and the extracellular matrix *in vivo* or their substratum *in vitro*.[52] Previous experiments with WEFF microscopy[38–44] have shown that focal contacts and adhesions are visualized. Moreover, an outline of the entire cell can be seen by acquiring data using high integration times due to an epi-fluorescence contribution from general scattering of the waveguide.[42] Here, we have chosen to acquire images in the evanescent mode with only small epi-fluorescence contributions to be able to identify single cells and colonies. Therefore, the Triton X-100 membrane interaction observed was predominantly within the first 70 nm above the waveguide and very close to focal adhesions.

Osteoblasts form bone by elaborating an extracellular matrix that then becomes mineralized.[53] Osteoblasts are derived from undifferentiated mesenchymal precursor cells that can also differentiate into several related cells types, including fibroblasts and chondrocytes. *In vivo*, osteoblasts are found on the surface of forming bone. Thus, adhesion of osteoblasts to the rigid waveguide surface *in vitro* mimics the adhesion of osteoblasts to the surface of bone *in vivo*. As osteoblasts are closely related to fibroblasts and several other connective tissue cells types, and

adhere to substrata via common mechanisms,[54] we expect that our results will be readily generalizable to many other cell types.

2 Materials and Methods

Ag^+-Na^+ ion-exchanged waveguides in SG11 glass (Schott, Grünenplan, Germany, refractive index, 1.513 at $\lambda =$ 543.5 nm) were used as the substrate for cell culture. Ion exchange was carried out in a pure $AgNO_3$ (99.0%, EMD, Gibbstown, NJ, USA) melt for 18 min at 275°C. By using a holography set-up, gratings with a periodicity of 650 to 685 nm in photoresist S1805 (Shipley Canada, Ottawa, Ontario, Canada) were fabricated on top of the waveguide and used to couple the laser beam into the waveguide. The stage of an inverted microscope (Axiovert 25, Zeiss, Oberkochen, Germany) was modified to accommodate the waveguide. The images were taken in TE polarization. The microscope is equipped with a 10×, 20×, and 63× objective lens. The images are taken with the 40× lens.

The MC3T3-E1 (Subclone 4) osteoblastic cell line was obtained from the American Type Culture Collection (Rockville, MD, USA). MC3T3-E1 cells are a clonal nontransformed cell line originally established from newborn mouse calvaria.[55] MC3T3-E1 cells were seeded on the waveguide in α-minimum essential medium (α-MEM) containing 15% heat-inactivated fetal bovine serum and antibiotics (penicillin 100 units/ml, streptomycin 100 μg/ml, and amphotericin B 0.25 μg/ml) (Invitrogen, Burlington, ON, Canada). After 24 h incubation, waveguides were washed with phosphate-buffered saline (PBS) to remove any nonviable cells. Cells were loaded with DiI, a lipophilic membrane stain that is weakly fluorescent until incorporated into membranes. Samples were incubated with 5 μM DiI in dimethyl sulfoxide ($DiIC_{18}(3)$ from Invitrogen) at 37°C for 20 min, followed by several washes with PBS. Cells were imaged in Dulbecco's Modified Eagle Medium (DMEM) without phenol red (Invitrogen). The excitation and emission wavelengths for DiI are 549 and 565 nm, respectively.

A cuvette made from blackened aluminum was sealed with an O-ring (Buna-N, McMaster Carr, Princeton, NJ) to the waveguide with loaded cells on its surface. Using a rotating and translating stage, the 543.5 nm laser beam was directed onto the coupling grating on the waveguides. At waveguide mode resonance angles, the laser beam coupled into the waveguide and an evanescent field was generated in the cover medium to excite the fluorophores in the plasma membrane nearest the waveguide surface. The light emitted from the fluorophores was collected by an objective. A 560-nm long pass filter (3DR560LP, Omega Optics, Brattleboro, VT) was used to block scattered excitation light. A digital camera (Diagnostic Instruments, Inc., Sterling Heights, MI) with imaging software (Image Pro Express, Media Cybernetics, Bethesda, MD) was used for capturing images. Image analysis was carried out using ImageJ software (National Institutes of Health, Bethesda, MD).

Images of the cell-substrate interface without the addition of detergent were captured to investigate photobleaching and to monitor possible morphological changes in cells in the absence of Triton X-100. Medium (phenol red-free DMEM) was then removed and replaced with the medium containing Triton X-100 at concentrations of 0.013, 0.1, 0.5 or 1.0 w/w%. Image capture resumed immediately after adding Triton X-100. Imaging continued until the cells were completely solubilized and fluorescence had completely disappeared. Using ImageJ, a sequence of images was obtained and the integrated intensities of individual cells or of cell colonies were measured and background subtracted. For determining the background intensity, the selected cell image area was moved to the nearest place on the image where no cells were located. There, the background intensity was measured for

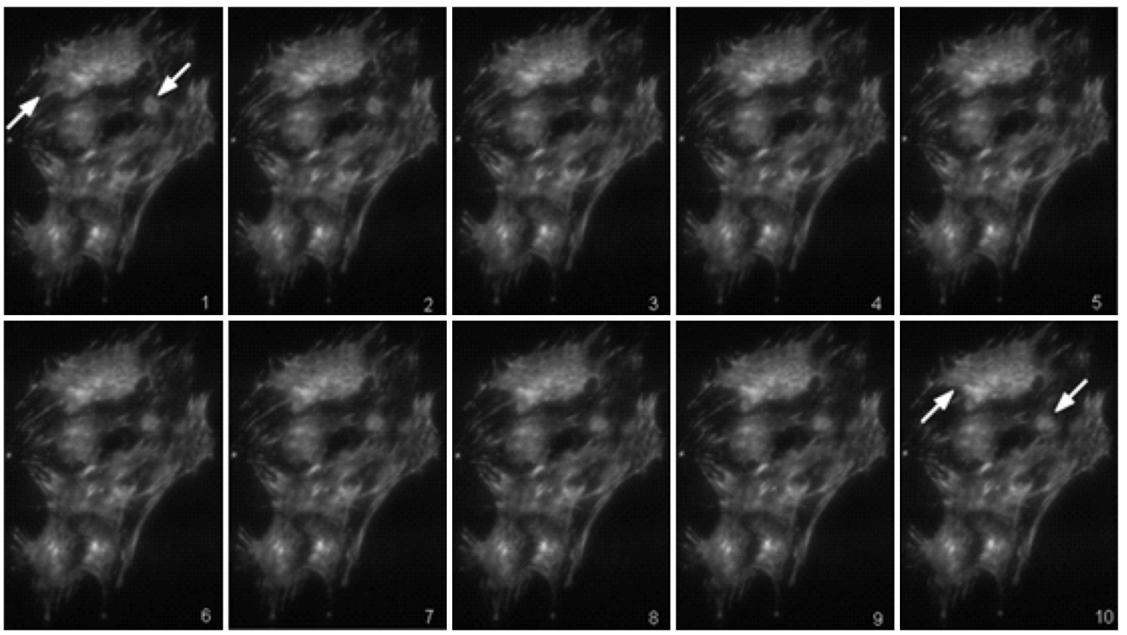

Fig. 2 Time sequence of WEFF microscopy images of live osteoblasts in the absence of Triton X-100. The time between the first and the last image was 23 min. Seen are focal adhesions and cell outlines visible due to some waveguide scattering and therefore a small epi-fluorescence contribution.[42] Locations marked with arrows on the images show minor changes in cell morphology. Image parameters: gain 2, integration time 1.4 s, width of image 75 μm, objective 40×. Data are representative of 3 independent experiments.

each image. Normalization for quantitative data was carried out as follows. Various cells in a single experiment were first imaged. Then using ImageJ, the integrated intensity in all cells was measured and normalized to cell area. All data were then normalized to the integrated intensity at $t = 0$.

3 Results and Discussion

3.1 *Photobleaching*

To quantitatively investigate intensity data with time, it needed to be established whether photobleaching was occurring. To investigate photobleaching and to track possible changes in cell morphology, images of DiI-labeled cells in the absence of Triton X-100 were captured with increasing time during continuous evanescent illumination (Fig. 2). In addition to focal adhesions, which were evident as bright spots, parts of cells outside the evanescent field were seen due to photons scattered by the waveguide, which leads to some epi-fluorescence background.[42] The integration time was chosen so that the epi-fluorescence contribution was small. The time sequence in Fig. 2 revealed only small changes in cell morphology over 23 min. The two arrows on the first and last images indicate regions of the cell membrane where changes are noticeable. The directions of the arrows show the directions of cell movement. However, the integrated intensity of cells in the absence of Triton X-100 remained constant (see Fig. 3), indicating that no photobleaching occurred.

3.2 *Solubilization of Cell Membrane with Triton X-100*

Cells were labeled with DiI and monitored using time-lapse WEFF microscopy. Plasma membrane solubilization was initiated by replacing medium with medium containing the detergent Triton X-100 (0.013 w/w%). In these experiments, a static sample chamber was used (i.e., no medium exchange was carried out during imaging), so that changes in fluorescence dye concentration in the medium due to release from cells was observed as a changing background signal. Figure 4 shows images during cell solubilization, a reaction taking approximately 1 h. The time increases in Fig. 4 with increasing image number. By following the arrow in the images with time, one can see how the plasma membrane close to a focal adhesion responded to Triton X-100. After adding detergent, the integrated image brightness first increased (Fig. 4, images 1 to 5, and Fig. 3). The increase in brightness lasted for about 7 min. Then, the intensity 'plateaued' for the next 7 min. Following approximately 14 min incubation with Triton X-100 (0.013 w/w%), the fluorescence intensity decreased, first rapidly then more slowly (Fig. 4 image 11 to 20; Fig. 3). Imaging continued until the cell image disappeared, at which point the plasma membrane appeared to be completely solubilized and disappeared out of the evanescent field.

To quantify the solubilization process, the integrated intensity of the images with time was measured using ImageJ

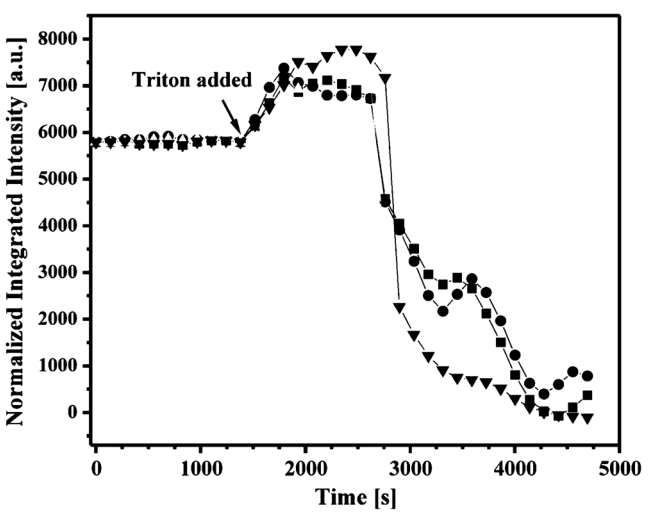

Fig. 3 Integrated intensities of three cells or cell colonies versus time (each indicated with a different symbol). Triton X-100 (0.013 w/w%) was added where indicated by the arrow. Prior to adding detergent, the integrated fluorescence intensities of the cells were constant indicating negligible photobleaching. After adding Triton X-100, the integrated intensity for all samples increased, "plateaued' and then decreased.

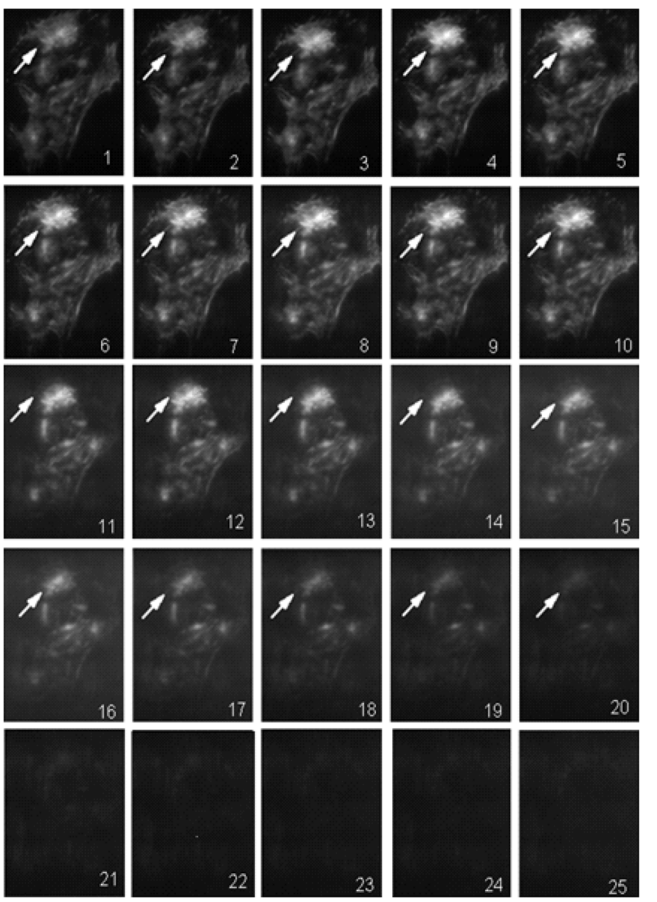

Fig. 4 Sequence of WEFF microscopy images of osteoblasts in the present of Triton X-100 (0.013 w/w%) within 1 h. The first row (images 1 to 5) of the images shows stage I, detergent uptake and fluorescence intensity increase. Row two (images 6 to 10) shows stage II, morphological change without micelles leaving (plateau with constant fluorescence intensity). Rows three to five (images 11 to 25) depict stage III, a decrease in fluorescence due to dispersal of micelles. Image parameters: gain 2, integration time 1.4 s, width 75 μm, objective 40×. Data are representative of 3 independent experiments.

software. For discrete cells or a small colony of cells, the area was selected and the integrated intensity was measured. Then the background signal was determined and subtracted to eliminate the contribution of fluorescence from dye dispersed upon Triton X-100 solubilization. In the absence of Triton X-100, the integrated intensities were constant (Fig. 3), confirming the stability of cells and the lack of photobleaching. Upon addition of Triton X-100, the integrated intensities first increased, and then 'plateaued.' This was followed by a biphasic decrease in fluorescence intensity, consisting of a rapid initial drop and a subsequent slow decrease to near background levels.

3.3 *Interpreting Cell Membrane Solubilization using the Three-Stage Model of Lipid-Detergent Interaction*

The three stage model of membrane-detergent interaction[8] was developed to describe solubilization of artificial membrane systems (liposomes and supported lipid bilayers) by various detergents.[8,28,56–58] Kinetic data describing liposome solubilization have been obtained from changes in turbidity or light scattering in liposome suspensions upon addition of detergent in increasing amounts. In the present study, kinetic data were derived from changes in the integrated intensity of the light emitted from a membrane-intercalated fluorophore upon addition of detergent.

Our kinetic data show integrated intensities from cells (the sum of evanescent and minor epi-fluorescence signals) with and without Triton X-100 (Fig. 3). In the absence of detergent, the integrated intensities are constant. In the presence of the detergent, three reproducible kinetic stages were found: (i) an increase in fluorescence intensity, (ii) a 'plateau', and (iii) a decrease in intensity. Therefore, a comparison to or an adaption of the established three-stage model is possible. In stage I, the membrane takes up detergent and the concentration of detergent rises in the plasma membrane. The integrated fluorescence intensity increases due to suppression of fluorophore quenching by dilution of the dye with detergent[58,59] in the cell membrane. (An alternative interpretation of the intensity increase would be movement of the dyes closer to the waveguide surface into higher evanescent fields. However, movement of the focal adhesions towards the waveguide is very unlikely.) In this stage, solubilization does not occur. According to the model, stage I ends when the membrane becomes saturated with detergent. The end of stage I is seen in Fig. 3 when the intensity increase ends and the plateau starts.

In stage II of artificial membrane solubilization, the detergent-saturated lipid bilayer undergoes a structural transition and converts partially into lipid-detergent mixed micelles; however, these micelles are not yet mobile, but still incorporated in the membrane. Therefore, stage II is seen in our data as the plateau in which intensity remains constant as the dye is not leaving the evanescent field. At this time, the dye is still located either in the membrane or in formed micelles in unquenched conditions mixed with detergent.

During stage III, the micelles become mobile and leave the evanescent field, leading to a decrease in integrated intensity. Individual micelles are too small to be seen with our WEFF microscope, a diffraction-limited technology.

If this 3-stage model is correct, then the background intensity determined by WEFF microscopy should not increase during stages I and II, as no dye molecules have yet left the membrane. On the other hand, background intensity should start to increase at the onset of stage III, when micelles begin to disperse. This is indeed observed. Figure 5 shows the raw data (integrated intensity of cells and background) and the difference (cell integrated intensity minus background integrated intensity) for three experiments carried out with increasing concentrations of Triton X-100 (0.1, 0.5 and 1.0 w/w%). Clearly, the background intensity starts to increase about the time at which stage II transitions into stage III.

Increasing the detergent concentration accelerated the solubilization process; all stages were shorter. At the lowest concentration of Triton X-100 (0.013 w/w%, Figs. 2 to 4), the entire process lasted ~3000 s (50 min), at 0.1 w/w% ~700 s

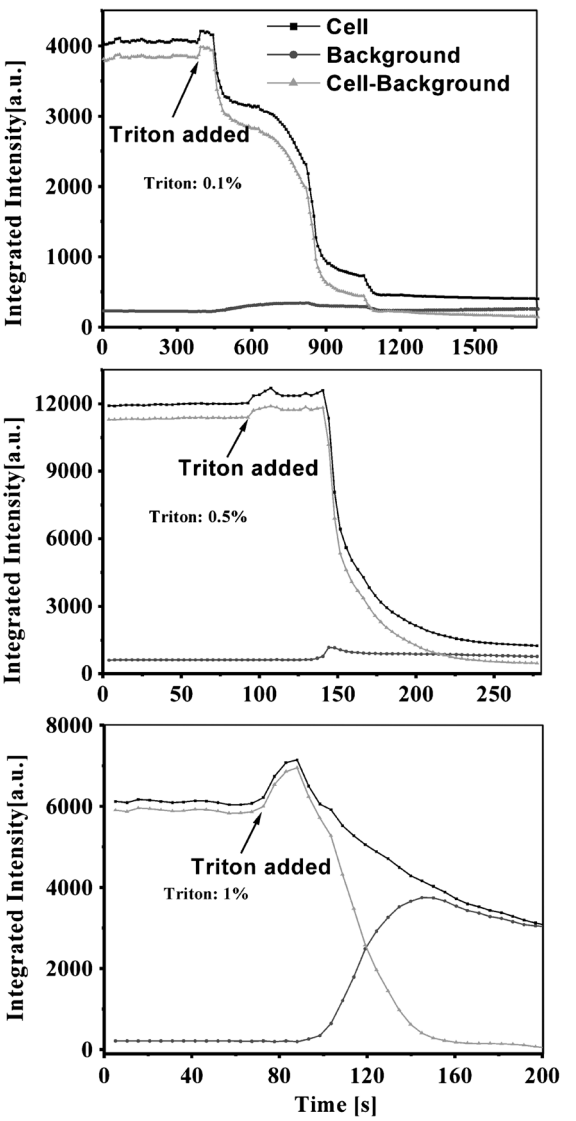

Fig. 5 Integrated intensities of three different cell samples and background versus time. Shown are the integrated fluorescence intensities of the (i) cell, (ii) background and (iii) cell minus background. Prior to adding detergent, the integrated fluorescence intensities of the cells, background and cell-background were constant. Triton X-100 (0.1, 0.5 or 1.0 w/w%) was added where indicated by the arrows. After adding Triton X-100, the integrated intensities increased, plateaued (for 0.1 and 0.5 w/w%) and then decreased. However, at 1.0 w/w%, the extended plateau stage was missing. Note the different time scales in each panel. Data are representative of three independent experiments.

(11 to 12 min), at 0.5 w/w% ~160 s (2.7 min), and at 1.0 w/w% ~100 s (1.7 min). Please note the different time scales in Fig. 5. The pattern of solubilization kinetics was similar at all concentrations. However, at the highest detergent concentration, the plateau was not prominent. It might be that, at this high concentration of Triton X-100, the transition between membrane and membrane-micelles started during stage I. Therefore, stage III (release of micelles) would begin very quickly after detergent uptake. The background data support this hypothesis, as the onset of the increase in background signal coincides with the time of peak intensity in Fig. 5 (lower panel).

At the beginning of micelle loss (start of stage III), the background signal shows fluorophore leaving the plasma membrane into the medium within the evanescent illumination volume. Later on during stage III, the background intensity reflects two processes: (i) increased concentration of fluorophore leaving the membrane due to solubilisation, and (ii) disappearance of the fluorophore and its host micelles from the evanescent test volume, due to dispersion into the medium. Therefore, the background signal increases upon membrane solubilization then decreases. The final value of the background signal should be larger than its initial value before detergent, due to homogeneous distribution of fluorophore-containing micelles in the medium.

The reason for the two time constants involved in the decrease in cell intensity in stage III may be a combination of two factors. The first is micelle dispersion as discussed above. The second is cell death and detachment. The cells are alive at the beginning of the experiment, but die during the course of detergent uptake. When cells die, they are not necessarily able to maintain adhesion to the substrate. Therefore, one of the two time constants may reflect loosening of focal adhesions, allowing cells to lift away from the waveguide surface and decreasing signal intensity. On the other hand, the pattern of changes in the background signal (described above) is consistent with the predominant factor being micelle dispersion.

4 Conclusion

WEFF microscopy was used to visualize the solubilization of plasma membranes of living osteoblasts close to their focal adhesions using Triton X-100 in an aqueous environment. Images and integrated intensities in the absence of Triton X-100 showed that the influence of photobleaching is negligible; therefore, experiments can be performed over extended periods of time. The results presented here for plasma membrane solubilization in live cells agree well with the results of studies on liposomes and supported lipid bilayers. A multistep process was observed. In the first stage, incorporation of Triton X-100 into the cell membrane resulted in an increase in image brightness due to a decrease in DiI quenching. After detergent saturation, an intensity plateau was observed, which we interpret as the time required for transition from a lipid bilayer to a membrane-micelle mixture. During the final stage, micelles became mobile and left the membrane, leading to a decrease in object intensity and an increase in the background signal. Increasing the concentration of Triton X-100 did not change the three-stage kinetics, but did decrease the duration of each stage.

In summary, we have shown that authentic plasma membranes in living osteoblasts behave in a similar way as model membrane systems, despite the presence of additional constituents (e.g., proteins, glycolipids, etc.), which are typically missing in model membranes. We expect that other cell types will behave in the same way as osteoblasts.

Acknowledgments

We thank Elizabeth Pruski (Western University) for expert assistance with cell culture and Bulent Mutus (Department of Chemistry and Biochemistry, University of Windsor) for helpful discussions about DiI quenching. We acknowledge the Western Nanofabrication Laboratory for hosting our laser holography equipment and for providing photoresist technology. S.M. gratefully acknowledges support from the Canada Research Chairs program. This project was funded by the Natural Sciences and Engineering Research Council of Canada (NSERC), Canada Foundation for Innovation (CFI) and the Ontario Innovation Fund (OIF).

References

1. L. Shapiro and R. M. Losick, Eds., *Cell Biology of Bacteria: A Subject Collection*, Cold Spring Harbor, New York (2011).
2. R. B. Gennis, *Biomembranes: Molecular Structure and Function*, Springer, New York (1989).
3. D. Q. Ni et al., "Isolation, folding and structural investigations of the amino acid transporter OEP16," *Protein Exp. Purif.* **80**(2), 157–168 (2011).
4. M. Valente et al., "Expression, purification, electron microscopy, N-glycosylation mutagenesis and molecular modeling of human P2X4 and Dictyostelium discoideum P2XA," *Biochim. Biophys. Acta-Biomembr.* **1808**(12), 2859–2866 (2011).
5. V. Teixeira, M. J. Feio, and M. Bastos, "Role of lipids in the interaction of antimicrobial peptides with membranes," *Prog. Lipid Res.* **51**(2), 149–177 (2012).
6. V. Lewis and N. M. Hooper, "The role of lipid rafts in prion protein biology," *Front. Biosci. Landmark* **16**, 151–168 (2011).
7. V. N. Ngassam et al., "A comparison of detergent action on supported lipid monolayers and bilayers, *Soft Matter* **8**(14), 3734–3738 (2012).
8. D. Lichtenberg, J. Robson, and E. A. Dennis, "Characterization of the solubilization of lipid bilayers by surfactants," *Biochim. Biophys. Acta* **821**(3), 470–478 (1985).
9. D. Lichtenberg, F. M. Goni, and H. Heerklotz, "Detergent-resistant membranes should not be identified with membrane rafts," *Trends Biochem. Sci.* **30**(8), 430–436 (2005).
10. S. Morandat and K. E. Kirat, "Solubilization of supported lipid membranes by octyl glucoside observed by time-lapse atomic force microscopy," *Colloids Surf. B Biointerfaces* **55**(2), 179–184 (2007).
11. M. L. Jackson et al., "Solubilization of phosphatidylcholine bilayers by octyl glucoside," *Biochemistry* **21**(19), 4576–4582 (1982).
12. D. Lichtenberg and Y. Zilberman, "Surface curvature and mobility in phospholipid bilayers. NMR studies of lecithin-deoxycholate mixed micelles," *J. Magn. Reson.* **34**(3), 491–497 (1979).
13. D. Lichtenberg et al., "Structural and kinetic studies on the solubilization of lecithin by sodium deoxycholate," *Biochemistry* **18**(16), 3517–3525 (1979).
14. C. Toroa et al., "Solubilization of lipid bilayers by myristyl sucrose ester: effect of cholesterol and phospholipid head group size," *Chem. Phys. Lipids* **157**(2), 104–112 (2009).
15. O. Lopez et al., "Structural modifications in the stratum corneum by effect of different solubilising agents: a study based on high-resolution low-temperature scanning electron microscopy," *Skin Pharmacol. App. Skin Phys.* **13**(5), 265–272 (2000).
16. U. Kragh-Hansen, M. le Maire, and J. V. Möller, "The mechanism of detergent solubilization of liposomes and protein-containing membranes," *Biophys. J.* **75**(6), 2932–2946 (1998).
17. A. de la Maza and J. L. Parra, "Solubilization of phospholipid bilayer caused by surfactants," *Am J. Oil. Chem. Soc.* **70**(7), 699–706 (1993).
18. M. le Maire, P. Champeil, and J. V. Möller, "Interaction of membrane proteins and lipids with solubilizing detergents," *Biochim. Biophys. Acta* **1508**(1), 86–111 (2000).

19. S. Schuck et al., "Resistance of cell membranes to different detergents," *Proc. Natl. Acad. Sci. U S A* **100**(10), 5795–5800 (2003).
20. H. K. Mangold, G. Zweig, and J. Sherma, Eds., Lipids CRC Press, Boca Raton, FL (1984).
21. S. Almog et al., "States of aggregation and phase transformation in mixtures of phosphatidylcholine and octyl glucoside," *Biochemistry* **29**(19), 4582–4592 (1990).
22. M. A. N. Partearroyo et al., "Solubilization of phospholipid bilayers by surfactants belonging to the Triton Xseries: effect of polar group size," *J. Colloid Inter. Sci.* **178**(1), 156–159 (1996).
23. M. Cocera et al., "Solubilization of stratum corneum lipid liposomes by Triton X-100. Influence of the level of cholesteryl sulfate in the process," *Colloids Surf. A Physicochem. Eng. Asp.* **182**(1–3), 15–23 (2001).
24. A. de la Maza and J. L. Parra, "Solubilizing effects caused by the nonionic surfactant dodecylmaltoside in phosphatidylcholine liposomes," *Biophys. J.* **72**(4), 1668–1675 (1997).
25. F. M. Goni and A. Alonso, "Spectroscopic techniques in the study of membrane solubilization reconstitution and permeabilization by detergents," *Biochim. Biophys. Acta* **1508**(1–2), 51–68 (2000).
26. K. Edwards et al., "Effects of Triton X-100 on sonicated lecithin vesicles," *Langmuir* **5**(2), 473–478 (1989).
27. A. de la Maza and J. L. Parra, "Vesicle- micelle structure transition of phosphatidylcholine bilayers and Triton X-100," *Biochem. J.* **303**(Pt. 3), 907–914 (1994).
28. O. Lambert et al., "A new gel-like phase in dodecyl maltoside–lipid mixtures: implications in solubilization and reconstitution studies," *Biophys. J.* **74**(2), 918–930 (1998).
29. S. Almog et al., "Kinetic and structural aspects of reconstitution of phosphatidylcholine vesicles by dilution of phosphatidylcholine-sodium cholate mixed micelles," *Biochemistry* **25**(9), 2597–2605 (1986).
30. M. L. Jackson and B. J. Litman, "Rhodopsin-egg phosphatidylcholine reconstitution by an octyl glucoside dilution procedure," *Biochim. Biophys. Acta* **812**(2), 369–376 (1985).
31. A. Helenius, M. Sarvas, and K. Simons, "Asymmetric and symmetric membrane reconstitution by detergent elimination. Studies with Semliki Forest virus spike glycoprotein and penicillinase from the membrane of *Bacillus licheniformis*," *Eur. J. Biochem.* **116**(1), 27–35 (1981).
32. N. A. Mazer, G. B. Benedek, and M. C. Carey, "Quasielastic light-scattering studies of aqueous biliary lipid systems. Mixed micelle formation in bile salt-lecithin solutions," *Biochemistry* **19**(4), 601–615 (1980).
33. D. Levy et al., "A systematic study of liposome and proteoliposome reconstitution involving bio-bead-mediated Triton X-100 removal," *Biochim. Biophys. Acta* **1025**(2), 179–190 (1991).
34. P. K. Vinson, Y. Talmon, and A. Walter, "Vesicle-micelle transition of phosphatidylcholine and octyl glucoside elucidated by cryo-transmission electron microscopy," *Biophys. J.* **56**(4), 669–681 (1989).
35. A. Walter et al., "Intermediate structures in the cholatephosphatidylcholine vesicle-micelle transition," *Biophys. J.* **60**(6), 1315–1325 (1991).
36. G. Csucs and J. J. Ramsden, "Solubilization of planar bilayers with detergent," *Biochim. Biophys. Acta* **1369**(2), 304–308 (1998).
37. A. Helenius and K. Simons, "Solubilization of membranes by detergent," *Biochim. Biophys. Acta* **415**(1), 29–79 (1975).
38. H. M. Grandin et al., "Waveguide excitation fluorescence microscopy: a new tool for sensing and imaging the biointerface," *Biosens. Bioelectron.* **21**(8), 1476–1482 (2006).
39. B. Agnarsson et al., "Evanescent-wave fluorescence microscopy using symmetric planar waveguides," *Opt. Express* **17**(7), 5075–5082 (2009).
40. A. Hassanzadeh et al., "Waveguide evanescent field fluorescence microscopy: thin film fluorescence intensities and its application in cell biology," *Appl. Phys. Lett.* **92**(23), 233503 (2008).
41. A. Hassanzadeh et al., "Multimode waveguide evanescent field fluorescence microscopy: measurement of cell-substratum separation distance," *Appl. Phys. Lett.* **94**(3), 033503 (2009).
42. A. Hassanzadeh et al., "Optical waveguides formed by silver ion exchange in Schott SG11 glass for waveguide evanescent field fluorescence microscopy: evanescent images of HEK293 cells," *J. Biomed. Opt.* **15**(3), 036018 (2010).
43. A. Hassanzadeh et al., "Waveguide evanescent field fluorescence microscopy: from cell-substratum distances to kinetic cell behaviour," *Proc. SPIE* **7322**, 73220A (2009).
44. A. Hassanzadeh and S. Mittler, "Waveguide evanescent field fluorescence microscopy: high contrast imaging of a domain forming mixed lipid Langmuir-Blodgett monolayer mimicking lung surfactant," *J. Biomed. Opt.* **16**(4), 046022 (2011).
45. H. Felix, "Permeabilized cells," *Anal. Biochem.* **120**(2), 211–234 (1982).
46. S. A. Taya and T. M. El-Agez, "A reverse symmetry optical waveguide sensor using a plasma substrate," *J. Opt.* **13**(7), 075701 (2011).
47. G. Li, F. Lai, and Y. Fang, "Modulating cell-cell communication with a high-throughput label-free cell assay," *J. Lab. Autom.* **17**(1), 6–15 (2012).
48. K. Cottier and R. Horvath, "Imageless microscopy of surface patterns using optical waveguides," *Appl. Phys. B* **91**(2), 319–327 (2008).
49. A. Aref et al., "Optical monitoring of stem cell-substratum interactions," *J. Biomed. Opt.* **14**(1), 010501 (2009).
50. I. Giaever and C. R. Keese, "A morphological biosensor for mammalian cells," *Nature* **366**, 591–592 (1993).
51. M. H. McCoy and E. Wang, "Use of electric cell-substrate impedance sensing as a tool for quantifying cytopathic effect in influenza, A virus infected MDCK cells in real-time," *J. Virol. Methods* **130**(1–2), 157–161 (2005).
52. B. Geiger and K. M. Yamada, "Molecular architecture and function of matrix adhesions," *Cold Spring Harb Perspect Biol.* **3**(5), 1 (2011).
53. S. Harada and G. A. Rodan, "Control of osteoblast function and regulation ofbone mass," *Nature* **423**, 349–355 (2003).
54. A. Shekaran and A. J. García, "Extracellular matrix-mimetic adhesive biomaterials for bone repair," *J. Biomed Mater. Res. A.* **96**(1), 261–272 (2011).
55. H. Sudo et al., "In vitro differentiation and calcification in a new clonal osteogenic cell line derived from newborn mouse calvaria," *J. Cell Biol.* **96**(1), 191–198 (1983).
56. J. L. Rigaud, B. Pitard, and D. Levy, "Reconstitution of membrane proteins into liposomes: application to energy-transducing membrane proteins," *Biochim. Biophys. Acta* **1231**(3), 223–246 (1995).
57. G. D. Eytan, "Use of liposomes for reconstitution of biological function," *Biochim. Biophys. Acta* **694**(2), 185–202 (1982).
58. J. R. Silvius, "Solubilization and functional reconstitution of biomembrane components," *Ann. Rev. Biophy. Biomol. Struct.* **21**, 323–348 (1992).
59. M. Morawitz, "Distance determination via waveguide evanescence field fluorescence microscopy," Master Thesis, (2012).